Pharmacological Research 225 (2026) 108121

Contents lists available at ScienceDirect

Pharmacological Research

journal homepage: www.elsevier.com/locate/yphrs

A resveratrol–hydrogen sulfide donor hybrid as a multi-target therapeutic strategy for allergic asthma

Martina Simonelli [a,1], Ida Cerqua [a,1], Danilo D'Avino [a], Elisabetta Granato [b], Alessandra Perrella [a], Sara Perna [a], Antonietta Rossi [a], Raffaele Capasso [c], Federica Sodano [a], Antonia Scognamiglio [a], Elisa Magli [d], Ferdinando Fiorino [a], Giuseppe Caliendo [a], Beatrice Severino [a], Angela Corvino [a,1], Fiorentina Roviezzo [a,*,1]

[a] Department of Pharmacy, School of Medicine and Surgery, University of Naples Federico II, Naples 80131, Italy
[b] Department of Genomic Medicine, The University of Texas MD Anderson Cancer Center, Houston, TX 77030, USA
[c] Department of Agricultural Sciences, University of Naples Federico II, Naples 80055, Italy
[d] Department of Public Health, School of Medicine, University of Naples Federico II, Via Pansini, 5, Napoli 80131, Italy

ARTICLE INFO

Keywords:
Airway remodeling
Resveratrol
Hydrogen sulfide
Asthma

ABSTRACT

Resveratrol (RESV) is a naturally occurring polyphenol with well-established antioxidant and anti-inflammatory properties, supporting its therapeutic potential in chronic respiratory diseases such as asthma. To enhance its efficacy, we developed a hybrid compound, R-TBZ, in which RESV is chemically linked to 4-hydroxythiobenzamide (TBZ), a slow-releasing hydrogen sulfide (H_2S) donor. This design aimed to improve chemical stability, bioavailability, and controlled activation while minimizing the toxicity associated with fast H_2S release. R-TBZ was synthesized via esterification of RESV with TBZ and showed high chemical stability, remaining over 95 % intact after 24 h under neutral and acidic conditions. Enzymatic hydrolysis occurred gradually ($t_{1/2} \approx 20$ h), releasing RESV as the sole detectable product. In allergen-challenged bronchial epithelial cells, R-TBZ demonstrated superior efficacy compared with RESV or TBZ alone. It enhanced mitochondrial antioxidant defenses, reduced mucus production, and suppressed pro-inflammatory cytokines (IL-6, IL-1β, and TNF-α). R-TBZ inhibited allergen-induced epithelial–mesenchymal transition and TGF-β–induced fibroblast activation, reducing α-SMA and vimentin expression more effectively than the parent compounds, indicating synergistic anti-remodeling activity. In a murine model of allergic asthma, R-TBZ improved lung function, reduced airway hyperresponsiveness, restored β_2-agonist responsiveness, and attenuated eosinophilic inflammation, Th2 cytokine production, and plasma IgE levels. Importantly, R-TBZ reversed airway structural remodeling, reducing peribronchial α-SMA expression and preserving epithelial and goblet cell morphology, effects not fully achieved by RESV alone. Overall, R-TBZ combines dual anti-inflammatory and anti-remodeling activities, overcoming key limitations of RESV and H_2S donors. This hybrid represents a promising multi-target therapeutic strategy for asthma, particularly for steroid-resistant airway remodeling.

1. Introduction

Resveratrol (RESV) is a naturally occurring polyphenolic compound found in various plant species, notably in the skin of grapes, berries, and peanuts [1]. RESV is a well-known nutraceutical compound with a broad spectrum of pharmacological activities [2]. It exerts a wide range of biological activities, with mounting evidence indicating its potent anti-inflammatory and antioxidant effects [3]. Numerous clinical trials have identified it as a promising therapeutic candidate for various diseases, including cardiovascular conditions, diabetes, neurodegenerative disorders, and respiratory ailments [4–6]. Furthermore, RESV and its analogs are pharmacologically safe and can be co-administered with other drugs to enhance therapeutic efficacy and reduce toxicity [7–9]. Despite these advantages, the practical application of RESV in both food and pharmaceutical industries remains limited. This is largely due to its poor bioavailability, low water solubility, and chemical instability [10,

* Corresponding author.
E-mail address: roviezzo@unina.it (F. Roviezzo).
[1] These authors contributed equally to this work

https://doi.org/10.1016/j.phrs.2026.108121
Received 19 December 2025; Received in revised form 28 January 2026; Accepted 28 January 2026
Available online 29 January 2026

11]. In biological systems, RESV is rapidly metabolized and excreted, which significantly limits its therapeutic potential. Specifically, it undergoes extensive first-pass metabolism in the liver and intestine via UDP-glucuronosyltransferase, resulting in the formation of glucuronic and sulfate conjugates, with resveratrol-3-O-glucuronide being the most abundant metabolite in both human and animal models [12,13]. This metabolic pathway substantially reduces RESV's bioavailability by limiting its permeability and promoting its excretion. Additionally, physicochemical characteristics hinder its clinical efficacy. It is susceptible to light, heat, and pH changes, and its low hydrosolubility necessitates the use of emulsifiers or stabilizers to achieve biologically active concentrations. Another major concern is whether RESV can accumulate in target tissues at sufficient bioactive levels. Circulating plasma concentrations are often barely detectable, particularly when administered in its free form, which is inherently poorly soluble and poorly absorbed [13]. Thus, high doses are required to achieve biological effects, but this increases the risk of side effects and metabolism. Overcoming these issues is key to unlocking its full therapeutic potential. Traditional approaches, such as nanoencapsulation, liposomal carriers, solid lipid nanoparticles, and multi-target strategies, have shown promise in improving its stability, solubility, and targeted delivery [10,14]. Among emerging alternatives, pulmonary administration stands out as a viable route, offering the potential to bypass first-pass metabolism and deliver therapeutically relevant concentrations directly to affected tissues, particularly in respiratory diseases. Several studies have explored this route using formulations such as resveratrol/β-cyclodextrin inclusion complexes, solid dispersions, and spray-dried powders for inhalation [15,16]. Notably, RESV loaded onto cholesterol-conjugated polyamidoamine nanoparticles significantly reduced inflammation in lung injury models, while hydroxypropyl-β-cyclodextrin (HP-β-CD) complexes improved resveratrol solubility and lung deposition [16].

Despite these advances, challenges remain, including formulation stability, optimal excipient concentrations, and consistent pharmacodynamic outcomes. To address these issues more effectively, the development of hybrid compounds, where RESV is chemically linked or co-formulated with other bioactive molecules, may offer synergistic benefits. Such hybrid designs could enhance bioavailability, protect against metabolic degradation, and simultaneously target multiple disease pathways. Therefore, this research could prioritize multifunctional delivery systems and hybrid compound strategies to fully realize therapeutic potential of resveratrol.

Here we have developed a new RESV hybrid compound, R-TBZ, in which 4-hydroxythiobenzamide (TBZ), a well-known hydrogen sulfide (H_2S) donor, is linked via an ester bond at the 4′-hydroxyl position of resveratrol. H_2S is an endogenously produced gaseous signaling molecule that plays a key regulatory role in various physiological and pathological processes, including inflammation, oxidative stress, and tissue remodeling. In asthma, emerging evidence suggests that H_2S acts as a protective mediator with significant anti-inflammatory and anti-remodeling properties. Specifically, H_2S has been shown to attenuate key features of airway remodeling such as airway smooth muscle (ASM) hypertrophy, subepithelial fibrosis, goblet cell hyperplasia, and epithelial–mesenchymal transition (EMT) [17]. However, clinical translation of H_2S-based therapies has been limited by the rapid release and poor bioavailability of conventional sulfide salts. To overcome these issues, slow-releasing H_2S donors, such as TBZ have been developed, offering improved pharmacokinetic profiles and sustained biological effects [18–20]. R-TBZ synthesis aims to enhance pharmacokinetic properties, such as chemical stability and oral bioavailability of RESV, while introducing H_2S-mediated anti-inflammatory/cytoprotective effects, potentially improving therapeutic outcomes. Here, we demonstrate that the conjugation of RESV with TBZ provides a dual mechanism of action, offering enhanced therapeutic potential in asthma treatment.

2. Materials and methods

2.1. Chemistry

2.1.1. General chemical synthesis

All reagents were commercial products purchased from Merck Life Science S.r.l. All reactions were carried out using a microwave oven (DISCOVER 2.0, CEM) especially designed for organic synthesis by placing the reagents and solvents in a sealed reactor specific for high-pressure reactions. All reactions were followed by TLC, carried out on Merck silica gel 60 F 254 plates with fluorescent indicator and the plates were visualized with UV light (254 nm). Solutions were dried over Na_2SO_4 and concentrated with a Buchi R-114 rotary evaporator at low pressure. Melting points were determined using a Buchi melting point M560 apparatus and are uncorrected. ^1H and ^{13}C NMR spectra were recorded on Brucher Advance 400 MHz instrument. All spectra were recorded in DMSO-d6. Chemical shifts are reported in ppm. The following abbreviations are used to describe peak patterns when appropriate: s (singlet), broad singlet (bs), d (doublet), doublet of doublets (dd), t (triplet), m (multiplet). Mass spectra of intermediates and final products were performed on LTQ Orbitrap XL™ Fourier transform mass spectrometer (FTMS) equipped with an ESI ION MAX™ (Thermo Fisher Scientific, Waltham, MA, USA) source operating in positive mode. MeOH was used as a solvent for compound infusion into LTQ Orbitrap source. 4-Carbamothioylbenzoic acid (TBZ-COOH): P_4S_{10} (300 mg, 1.35 mmol) was added to cold EtOH (5 mL) and the solution was placed in a 10 mL closed reaction vessel and prestirred for 10 min. Then, 4-cyanobenzoic acid (1, 99 mg, 0.675 mmol) was added in one portion and the closed reaction vessel was placed in the cavity of a CEM microwave reactor, run under pressure and irradiated according to the following parameters: T, 80 °C; ramp time, 2 min; hold time, 1.5 h; pressure, 150 psi; power, 150 W. The reaction mixture was poured into ultrapure ice-water, and the resulting precipitation was filtered off. The collected solid was then dissolved in EtOAc and subjected to washing with $NaHCO_3$. After removing the organic layer, the aqueous phase was acidified with HCl (pH 1–2) (10 mL) and subsequently extracted with EtOAc (25 mL) and brine (5 mL), followed by drying over anhydrous Na_2SO_4. The solvent then evaporated under vacuum, yielding the desired product, which was used as obtained without further purification. Yield: 97 %, yellow solid. ESI-MS $(M+H)^+$ *m/z* calcd. 181.2 for $C_8H_7NO_2S$; found 181.9. ^1H NMR (400 MHz, DMSO-d6) δ 13.18 (bs, 1 H), 10.05 (s, 1 H), 9.65 (s, 1 H), 7.91–7.99 (m, 4 H). ^{13}C NMR (100 MHz, DMSO-d6) δ 199.93, 167.23, 143.72, 133.07, 129.36, 127.81. R-TBZ: A suspension of resveratrol (100 mg, 0.438 mmol) in anhydrous tetrahydrofuran (5 mL) was placed in a 10 mL closed reaction vessel and TBZ-COOH (71 mg, 0.482 mmol), EDAC·HCl (92 mg, 0.482 mmol), DMAP (55 mg, 0.482 mmol) were added. The closed reaction vessel was placed in the cavity of a CEM microwave reactor, run under pressure and irradiated according to the following parameters: T, 70 °C; ramp time, 2 min; hold time, 1 h; pressure, 150 psi; power, 100 W. After cooling to room temperature, the solvent was evaporated by distillation at reduced pressure in an amber round bottom flask to protect it from light. The crude material was purified by Biotage® ISOLERA flash chromatography (acetonitrile (ACN)+ 0.1 % trifluoroacetic acid (TFA)/water+ 0.1 % TFA 11:89 v/v to 100:0 v/v. Yield 32 %. mp. 194.5–195.8 °C. ESI-MS $(M+H)^+$ *m/z* calcd. 391.1 for $C_{22}H_{17}NO_4S$; found 392.2. ^1H NMR (400 MHz, DMSO-d6)δ 10.14 (s, 1 H), 9.80 (s, 1 H), 9.75 (s, 1 H), 9.61 (s, 1 H), 9.28 (s, 2 H), 8.16 (dd, $J = 8.3$, 6.4 Hz, 2 H), 8.03 (d, $J = 7.8$ Hz, 2 H), 7.69 (d, $J = 8.7$ Hz, 1 H), 7.43 (d, $J = 8.6$ Hz, 1 H), 7.31 (d, $J = 8.6$ Hz, 1 H), 7.15–7.09 (m, 2 H), 6.98–6.93 (m, 1 H), 6.86 (s, 1 H), 6.77 (d, $J = 8.6$ Hz, 1 H), 6.56 (t, $J = 2.0$ Hz, 1 H), 6.47 (d, $J = 2.0$ Hz, 2 H), 6.18 (t, d, $J = 2.0$ Hz, 1 H). ^{13}C NMR (100 MHz, DMSO-d6)δ ^{13}C NMR (101 MHz, DMSO) δ 199.66, 164.55, 164.46, 159.03, 158.89, 157.97, 152.17, 150.28, 144.58, 144.55, 140.32, 139.13, 135.57, 131.25, 131.14, 129.96, 129.91, 129.79, 128.53, 128.27, 128.10, 127.99, 127.35, 124.82, 122.58, 116.03, 110.17,

Table 1
List of primers.

Genes	Species	NCBI ID	Primer sequences	Tm (°C)
SOD-2	Human	6648	Forward: 5' – CTGGACAAACCTCAGCCCTAAC - 3'	**57.7**
			Reverse: 5' – AACCTGAGCCTTGGACACCAAC - 3'	**59.8**
GPXI	Human	2876	Forward: 5'- GTGCTCGGCTTCCCGTGCAAC - 3'	**63.8**
			Reverse: 5'- CTCGAAGAGCATGAAGTTGGGC - 3'	**58.3**
TNF-α	Human	7124	Forward: 5' – CTCTTCTGCCTGCTGCACTTTG – 3'	**58.8**
			Reverse: 5' – ATGGGCTACAGGCTTGTCACTC – 3'	**59.2**
IL-6	Human	3569	Forward: 5' - AGACAGCCACTCACCTCTTCAG – 3'	**58.5**
			Reverse: 5' - TTCTGCCAGTGCCTCTTTGCTG – 3'	**60.2**
IL-1β	Human	3553	Forward: 5' - CCACAGACCTTCCAGGAGAATG – 3'	**57.3**
			Reverse: 5' - GTGCAGTTCAGTGATCGTACAGG - 3'	**57.6**
MUC5AC	Human	4586	Forward: 5' - CCACTGGTTCTATGGCAACACC – 3'	**58.2**
			Reverse: 5' - GCCGAAGTCCAGGCTGTGCG – 3'	**63.8**
VIMENTIN	Human	7431	Forward: 5' - AGGCAAAGCAGGAGTCCACTGA - 3'	**60.8**
			Reverse: 5' - ATCTGGCGTTCCAGGGACTCAT – 3'	**60.4**
ACTA2	Human	59	Forward: 5' – CATCATGCGTCTGGATCTGG – 3'	**55.7**
			Reverse: 5' – GACAATCTCACGCTCAGCAG - 3'	55.9
β-ACTIN	Human	60	Forward: 5' - CACCATTGGCAATGAGCGGTTC - 3'	**59.3**
			Reverse: 5' - AGGTCTTTGCGGATGTCCACGT - 3'	**61.1**
Vimentin	Mouse	22343	Forward: 5' - CGGAAAGTGGAATCCTTGCAGG - 3'	**58.4**
			Reverse: 5' - AGCAGTGAGGTCAGGCTTGGAA - 3'	**60.8**
Acta2	Mouse	11475	Forward: 5' - TGCTGACAGAGGCACCACTGAA – 3'	**60.9**
			Reverse: 5' - CAGTTGTACGTCCAGAGGCATAG – 3'	**57.1**
β-actin	Mouse	11461	Forward: 5' - CATTGCTGACAGGATGCAGAAGG - 3'	**58.3**
			Reverse: 5' - TGCTGGAAGGTGGACAGTGAGG - 3'	**61.2**

108.15, 105.21.

2.1.2. Chemical stability

Experiments were performed as previously described with minor modifications [21]. Briefly, R-TBZ was first dissolved in DMSO and then diluted in phosphate-buffered saline (PBS, pH 7.4, 50 mM) or simulated gastric fluid without pepsin (SGF, pH 1.2), previously prepared according to standard protocols [22]. The final concentration of R-TBZ was adjusted to 39.11 ppm in all samples. Solutions were prepared in triplicate in glass tubes and incubated at 37 ± 0.5 °C for 24 h. At defined time intervals, 20 μL aliquots were withdrawn and directly analyzed by UHPLC as detailed in the following section. The experiments were conducted on a preparative scale (5 mL total volume), and aliquots were not replenished after sampling. Chemical stability data were used to determine the pseudo-first-order degradation kinetics of R-TBZ. Half-lives ($t_{½}$) were calculated from the linear regression of the logarithm of the remaining compound versus time. All experiments were carried out in triplicate, and results are reported as mean values.

2.1.3. Enzymatic stability

Experiments were carried out as previously described [23]. Briefly, a solution of R-TBZ in DMSO (1000 ppm) was added to a 3 % BSA solution in PBS, preheated to 37 °C. The resulting solutions (final concentration: 78.22 ppm) were maintained at 37 ± 0.5 °C. At predetermined time intervals, 300 μL aliquots were withdrawn and mixed with 300 μL of acetonitrile containing 0.1 % trifluoroacetic acid to deproteinize the medium. The samples were then sonicated using a Branson 2210 Ultrasonic Cleaner, vortexed with a Vortex ZX4 shaker equipped with an infrared system (Hosmotic, Naples, Italy) and centrifuged at 2150 *g* for 10 min using an Allegra X-30R refrigerated centrifuge (Beckman Coulter, Brea, CA, USA) equipped with fixed-angle rotors. The resulting clear supernatants were filtered through 0.45 μm PTFE filters (Alltech). From each sample, a 20 μL aliquot was withdrawn and analyzed by UHPLC, as described below. Enzymatic stability studies were conducted on a larger scale (5 mL), and aliquots were not replenished after sampling. All experiments were performed in at least triplicate. Data from enzymatic stability tests were used to determine the pseudo-first-order degradation kinetics of R-TBZ. Half-lives ($t_{½}$) were calculated from the linear regression of the logarithm of the remaining compound concentration versus time.

2.1.4. UHPLC analysis

Reverse-phase UHPLC was employed for the separation and quantification of the molecular hybrid R-TBZ and its corresponding metabolites, RESV and TBZ. Analyses were carried out using an Agilent 1260 PRIME Infinity II UHPLC system (Agilent Technologies, Palo Alto, CA, USA), equipped with a quaternary flexible pump (model G7104C), membrane degasser (model G1328C), diode-array detector (DAD, model G7115A), and a fluorescence detector (FLD, model G7121B), all integrated within the UHPLC 1260 Infinity II system. Data acquisition and processing were performed using OpenLab LC ChemStation software (Agilent Technologies). Chromatographic separation was achieved on a Poroshell 120 EC-C18 column (150 × 3.0 mm, 2.7 μm particle size, Agilent Technologies), maintained at room temperature. The mobile phase consisted of solvent A (water with 0.1 % TFA) and solvent B (acetonitrile with 0.1 % TFA), applied in a linear gradient from 10 % to 90 % B over 20 min. The flow rate was set at 0.5 mL/min, with an injection volume of 20 μL. After each run, the column was re-equilibrated for 4 min. Detection was performed at 230, 254, and 300 nm, with 800 nm used as a reference wavelength, selected according to the spectroscopic characteristics of each analyte. Quantification was carried out using calibration curves constructed over a concentration range of 0.78–50 ppm, with all curves demonstrating strong linearity ($r^2 > 0.99$).

2.2. In vitro studies

2.2.1. Cell culture

Monocyte/macrophage J774 (TIB 67, passage number twenty), bronchial epithelial cells BEAS-2B (CRL-9609 passage number six), and fibroblasts NIH-3T3 (CRL-1658 passage number twelve) were obtained from American Type Culture Collection (ATCC), and grown in adhesion in Dulbecco's modified Eagles medium (DMEM) supplemented with glutamine (2 mM, Aurogene Rome, Italy), Hepes (25 mM, Aurogene Rome, Italy), penicillin (100 U/mL, Aurogene Rome, Italy), streptomycin (100 μg/mL, Aurogene Rome, Italy), fetal bovine serum (FBS, 10 %, Aurogene Rome, Italy) and sodium pyruvate (1.2 %, Aurogene Rome, Italy) (DMEM completed). The cells were plated at a density of 1×10^6 cells in 75 cm^2 culture flasks and maintained at 37°C under 5 % CO_2 in a humidified incubator until 90 % confluence. The culture medium was changed every 2 days. Before a confluent monolayer appeared, sub-culturing cell process was carried out.

2.2.2. Cell treatment

After 24 h of serum starvation (DMEM supplemented with 0.1 % FBS), BEAS-2B cells were pretreated for 2 h with RESV (10 μM), TBZ

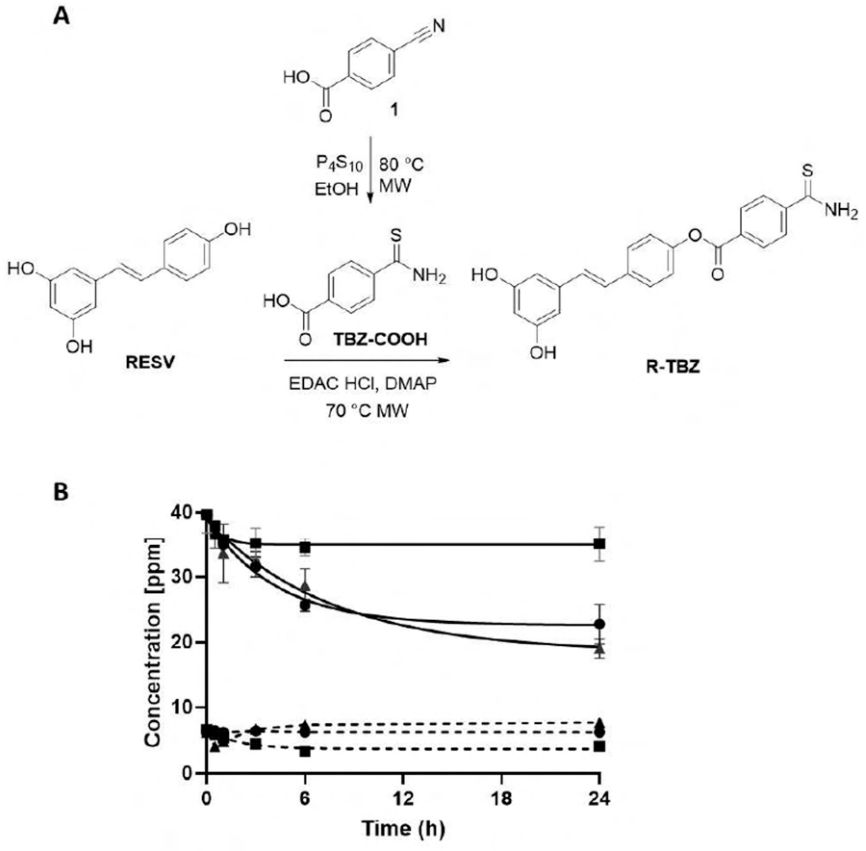

Fig. 1. Synthesis and stability of R-TBZ. **(A)** Synthetic strategies of R-TBZ. **(B)** Chemical and enzymatic stability of R-TBZ at 37°C. The figure reports the percentage of intact R-TBZ (solid lines) and the corresponding amount of released Resveratrol (RESV, dashed lines) over time in three different media: simulated gastric fluid without pepsin (SGF, pH 1.2, red), phosphate-buffered saline (PBS, pH 7.4, green), and bovine serum albumin (BSA, black). Results are expressed as mean values ± standard deviation (n = 3).

(10 μM), R-TBZ (10 μM), or vehicle (0.5 % DMSO). Cells were then stimulated for 24 h with *Dermatophagoides pteronyssinus* recombinant antigen Der P 1 (10 ng/mL; MyBioSource, MBS485103). The concentrations were selected based on literature as effective doses that do not induce cytotoxicity and are considered safe in BEAS-2B and comparable epithelial cell models. NIH-3T3 cells were pretreated for 2 h with RESV (10 μM), TBZ (10 μM), R-TBZ (10 μM), or vehicle (0.5 % DMSO). Cells were then stimulated for 48 h with 10 μg/mL of recombinant human TGF-beta 1 protein (TGF-β) (Abcam, AB500036). J774 cells were pretreated for 2 h with RESV (1, 3 and 10 μM), TBZ (1,3 and 10 μM), R-TBZ (1,3 and 10 μM), or vehicle (0.5 % DMSO) and then stimulated with 10 μg/mL of lipopolysaccharide (LPS) from *Escherichia coli* for 24 h [18].

2.2.3. Cell viability

Cell viability was assessed by the mitochondrial-dependent reduction of MTT (Sigma Aldrich, Milan, Italy) to formazan. J774 cells were plated to a seeding density of 1.0×10^5 in 96 multiwells. After incubation with the test compound for 24 h, cells were incubated in 96-well plates with MTT (0.2 mg/mL), for 1 h. The culture medium was removed, and the cells were lysed in dimethyl sulfoxide (DMSO; 0.1 mL). The extent of reduction of MTT to formazan within cells was quantified by the measurement of OD_{550}.

2.2.4. Prostaglandin and nitrite assay

After 24 h of incubation with LPS, the supernatants were collected for the measurement of prostaglandin (PG)E_2 (Cayman Chemical, VinciBiochem, Vinci, Italy) by ELISA assay. The nitrite concentration in the samples was measured by the Griess reaction, by adding 100 μL of Griess reagent (0.1 % naphthylethylenediamide dihydrochloride in H_2O and 1 % sulphanilamide in 5 % concentrated H_3PO_4; vol. 1:1; Sigma Aldrich, Milan, Italy) to 100 μL of samples. The optical density at 540 nm (OD_{540}) was measured immediately after Griess reagent addition, using ELISA microplate reader (Thermo Scientific, Multiskan GO). Nitrite concentration was calculated by comparison with OD_{540} of standard solutions of sodium nitrite prepared in culture medium.

2.2.5. Quantitative real-time PCR analysis

Total RNA was extracted from the BEAS-2B cells and NIH-3T3 cells were homogenized in Purezol Reagent (Bio-Rad, Hercules, CA) and RNA was extracted according to manufacturer's instructions. The quantification and quality analysis of RNA was ascertained by using NanoDrop™ One/OneC Microvolume UV-Vis Spectrophotometer (ThermoFisher Scientific, Monza, Italy). cDNA was synthesized by reverse transcription of 1 μg of RNA using the QuantiTect Reverse Transcription Kit (QIAGEN). Reverse transcription polymerase chain reaction (qRT–PCR) was performed by using Fast SYBR Green Master Mix (Applied Biosystem, Carlsbad, CA) and reactions were performed and analyzed on CFX Connect Real-Time PCR Detection System (Bio-Rad, Hercules, CA). Target genes expression calculations were normalized on reference housekeeping gene β-actin and expressed by using the $2^{-\Delta Ct}$ formula. Primers used are summarized in Table 1.

2.2.6. Immunofluorescence analysis

Cells were seeded onto glass coverslips (12 mm diameter) placed in 12-well plates at a density of 1×10^4 cells per well and allowed to adhere for 24 h at 37 °C in a humidified atmosphere containing 5 % CO_2. Then, cells were fixed in 4 % formaldehyde for 20 min at room temperature (RT). To eliminate any free aldehyde groups, cells were incubated with

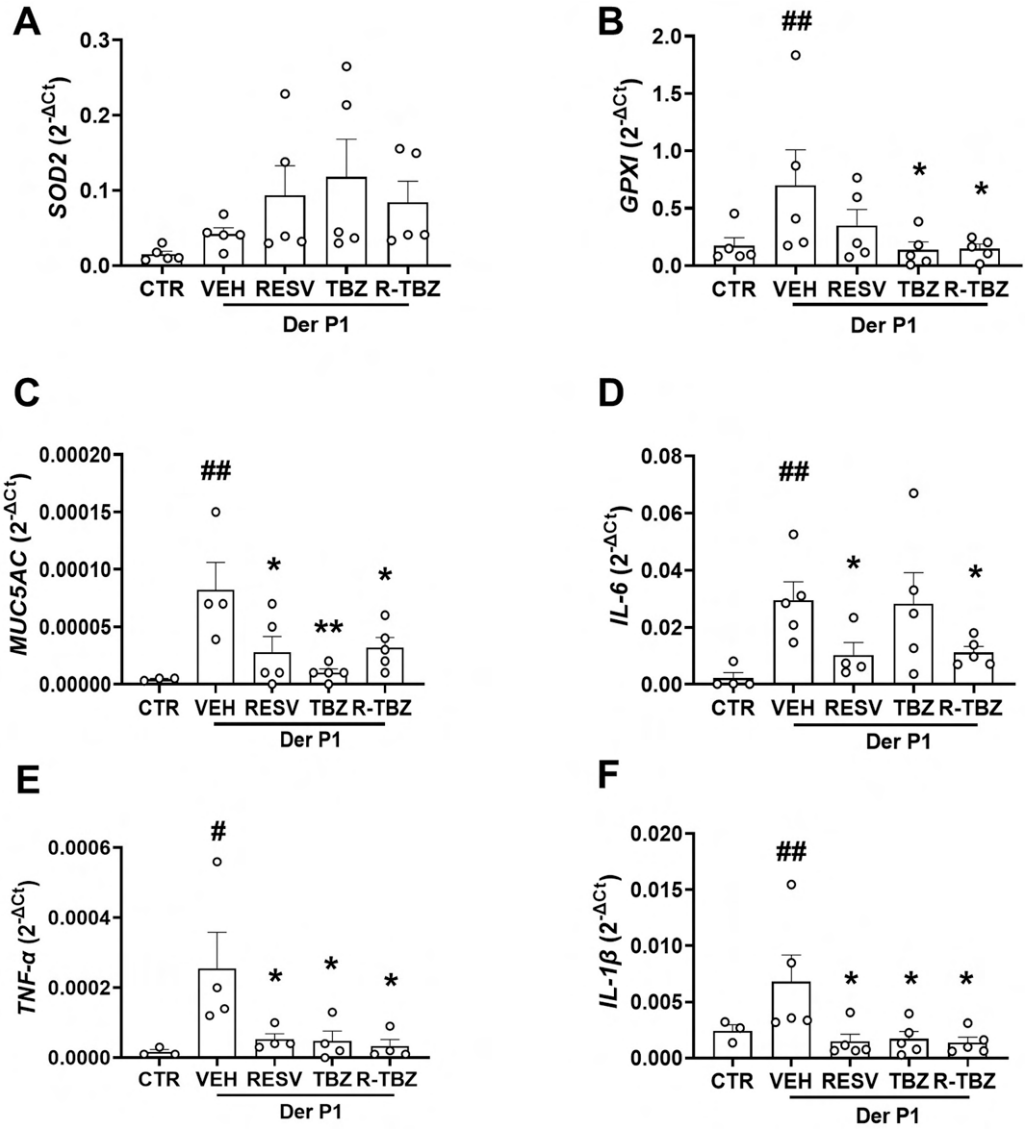

Fig. 2. R-TBZ modulates oxidative stress response, mucin production, and cytokine expression in allergen-stimulated bronchial epithelial cells. BEAS-2B bronchial epithelial cells were pretreated for 2 h with R-TBZ (10 μM), or parent compounds (RESV and TBZ; 10 μM) or vehicle (VEH) and then stimulated with Der P1 (10 ng/mL, 24 h). RT-PCR was utilized to assess gene expression levels of **(A)** *SOD2*, **(B)** *GPXI*, **(C)** *MUC5AC*, **(D)** *IL-6*, **(E)** *TNF-α* and **(F)** *IL-1β*. Data are expressed as mean ± S.E.M.; n = 5 for each group. $^{\#}p < 0.05$, $^{\#\#}p < 0.01$ *versus* untreated cells (CTR); *p < 0.05, **p < 0.01 *versus* vehicle (VEH); Statistical analysis used: ordinary one-way ANOVA plus Dunnett's *post hoc* test.

50 mM NH_4Cl for 30 min and then permeabilized with PBS 1X + 0.1 % Triton X-100 for 30 min at RT. Non-specific binding sites were blocked with 1X PBS + 1 % BSA. Anti-Vimentin (1:100; Abcam, ab92547) or anti-actin α-smooth muscle antibody (α-SMA; 1:100; Sigma-Aldrich, A5228) were incubated overnight at 4 °C. Goat anti-Rabbit IgG (1:1000; Invitrogen, A-11008) or goat anti-mouse IgG (1:1000; Invitrogen, A28175) were incubated 1 h at RT, and DAPI (1:5000; Sigma-Aldrich, D9542) was used to counterstain the nuclei. Images were acquired by ZEISS LSM 800 microscope with a magnification of 40x. Semi-quantitative determination was obtained with ImageJ/Fiji software measuring fluorescent intensity/number of nuclei.

2.3. In vivo studies

2.3.1. Animal modes

Female BALB/c mice (20 g, 8 weeks, Charles River Laboratories) were fed with standard rodent chow and water and acclimated for 4 days at a 12 h light and 12 h dark schedule in a constant air-conditioned environment (21 ± 2°C). Mice were blindly randomized into groups (n = 5 for each group), and experiments were carried out during the light phase. Experimental procedures were conducted in conformity with Italian (D.L. 26/2014) and European (Directive 2010/63/EU) regulations on the protection of animals used for scientific purposes and approved by the Italian Ministry (number: 896/2021-PR). The animal experiments also complied with ARRIVE (Animal Research: Reporting of In Vivo Experiments) guidelines, WMA Statement on animal use in biomedical research and recommendations of Association for Assessment and Accreditation of Laboratory Animal Care (AAALAC).

BALB/c mice were pre-treated with RESV (10 mg/kg; 0,00087 nmols), 4-hydroxy-thiobenzamide (TBZ, 5 mg/kg; 0.00068 nmols), R-TBZ (5 mg/kg or 10 mg/kg; 0.00029 and 0.00061 nmols), or vehicle (0.01 %DMSO in saline). Doses were selected based on the literature and on reported safety profiles, and the lowest effective dose was chosen to facilitate the detection of potential improvements in efficacy associated with the R-TBZ derivative. Ten minutes after pretreatment, mice were sensitized by subcutaneous injection (s.c.; 0.4 mL) of a suspension

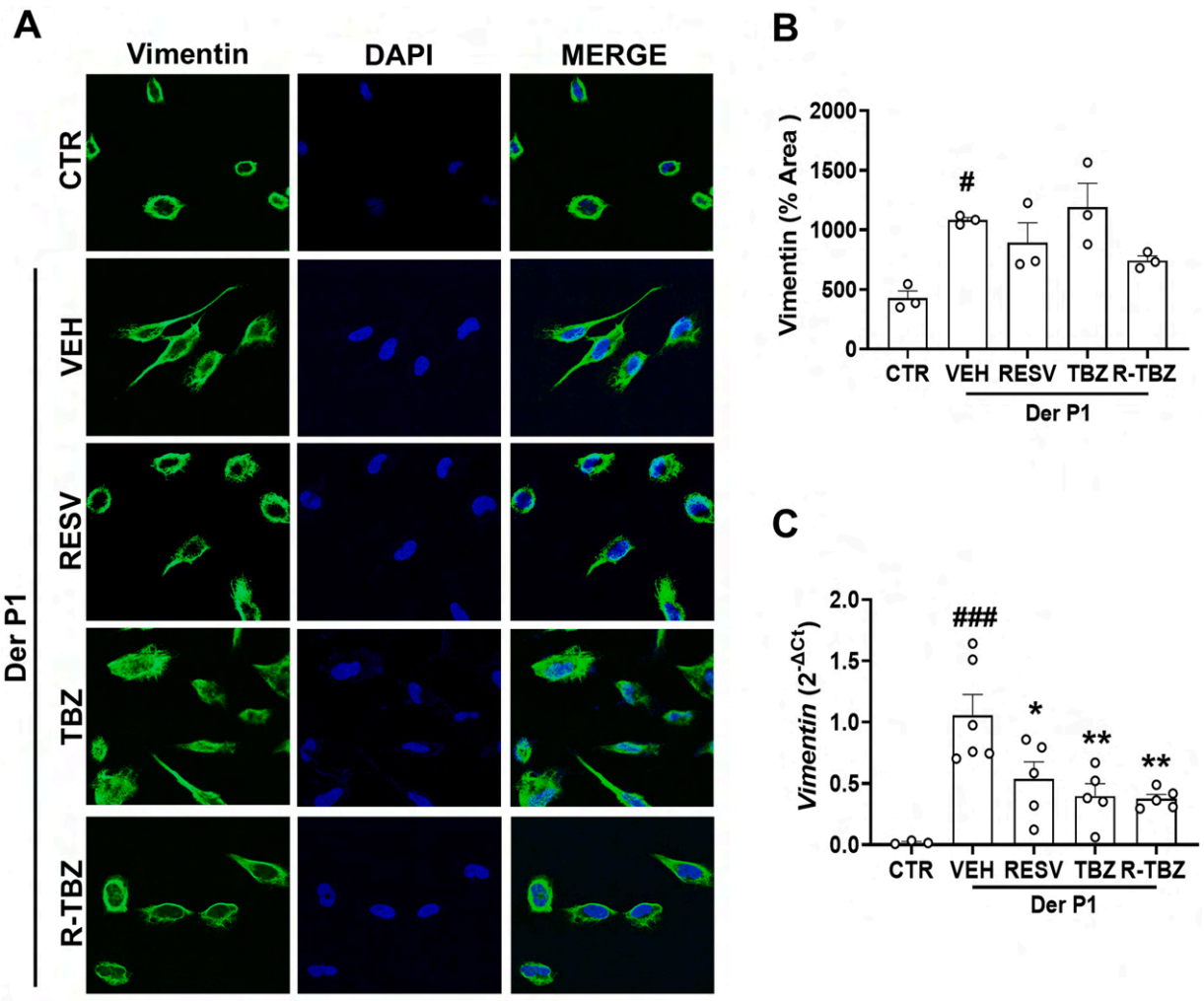

Fig. 3. R-TBZ inhibits allergen-induced EMT marker expression in allergen-stimulated bronchial epithelial cells. BEAS-2B bronchial epithelial cells were pretreated for 2 h with R-TBZ (10 μM), the parent compounds (RESV and TBZ; 10 μM) or vehicle (VEH) and then stimulated with Der P1 (10 ng/mL, 24 h). **(A)** Representative immunofluorescence staining for vimentin localization (40x objective). **(B)** Semi-quantitative determination (ImageJ/Fiji software) for vimentin. **(C)** RT-PCR analyses ($2^{-\Delta Ct}$) for the expression of vimentin-codifying gene. Data are expressed as mean ± S.E.M.; n = 3 **(A, B)** and n = 5 for each group **(C)**. $^{\#}p < 0.05$, $^{\#\#\#}p < 0.001$ *versus* untreated cells (CTR); $^{**}p < 0.01$ *versus* vehicle (VEH). Statistical analysis used: ordinary one-way ANOVA plus Dunnett's *post hoc* test.

containing 100 μg of ovalbumin from chicken egg white (OVA Grade V; Sigma-Aldrich, Milan, Italy) adsorbed to 13.3 mg of aluminum hydroxide (Merck KGaA, Darmstadt, Germany). All animals were sacrificed on day 21 by an overdose of enflurane, and lungs, bronchi, and blood were collected for functional and molecular analyses.

2.3.2. *Bronchial reactivity*

Bronchial tissues were dissected from mice and placed in isolated organ bath containing Krebs solution, at 37°C, oxygenated (95 % O_2 and 5 % CO_2), and connected to an isometric force transducer (type 7006, Ugo Basile, Comerio, Italy) associated to a Powerlab 800 (AD Instruments). Bronchi were initially stretched until a resting tension of 0.5 g was reached and allowed to equilibrate for at least 30 min. Tension was adjusted, when necessary, to 0.5 g and the bathing solution was periodically changed. Bronchial ring was exposed to a concentration-dependent curve of a β_2-agonist salbutamol (1×10^{-9} M – 3×10^{-5} M) or resveratrol (1×10^{-9} M – 3×10^{-5} M), or carbachol (1×10^{-9} M – 3×10^{-6} M). Results are expressed as dyne/mg tissue [18].

2.3.3. *Histological analysis*

Left lung lobes harvested from mice were fixed in formalin 4 %, embedded in paraffin and 6 μm sections were cut. Lung slices were processed to remove paraffin,rehydrated, and stained with Hematoxylin and eosin (H&E, Kaltek, Padua, Italy) to evaluate lung structure or with Periodic Acid-Schiff (PAS^+) to evaluate mucus production. For H&E protocol, lung slices were incubated with hematoxylin (8 min) rinsed in distilled water and then incubated in eosin solution 0.25 % for 10 s. For PAS^+ staining, slices were incubated in Periodic Acid solution 0.5 % for 10 min, rinsed in distilled water and then incubated with Shiff reagent for 15 min in the dark. Lung inflammation was evaluated using the Ashcroft Score, which ranges from 0 (no inflammation) to 4 (severe inflammation). Inflammation was graded based on epithelial damage, alveolar septal thickening, and eosinophilic infiltration. Images were evaluated independently, and scores were assigned without knowledge of group allocation. Images were acquired with Leica DM RB microscope (Leica, Milan, Italy) using a 10x and 20x objectives.

2.3.4. *Immunohistochemical analysis*

Other slices were processed for immunohistochemistry analysis and incubated with 3 % hydrogen peroxide (Sigma-Aldrich) for 15 min to quench the endogenous peroxidase activity. Non-specific interactions were reduced with 3 % BSA in PBS + 0.1 % Tween, and tissue sections were incubated overnight with anti-actin α-smooth muscle antibody (α-SMA; 1:100; Sigma, A5228) dissolved in 3 % BSA in PBS-0.1 % Tween or 3 % BSA in PBS-0.1 % Tween for negative control. After rinsing with PBS 0.01 M, sections were incubated with Peroxidase AffiniPure Goat

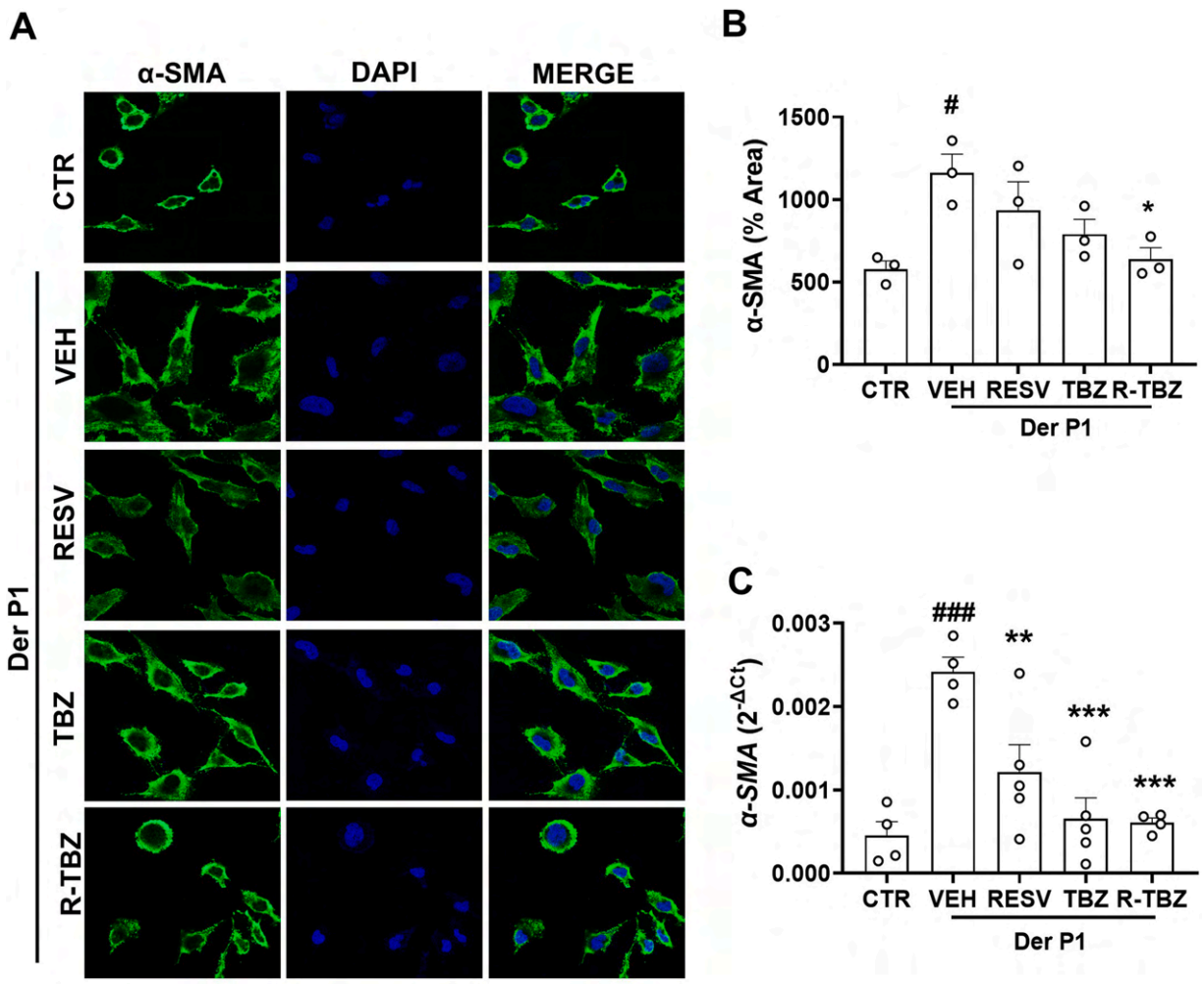

Fig. 4. R-TBZ inhibits allergen-induced remodeling marker expression in allergen-stimulated bronchial epithelial cells. BEAS-2B bronchial epithelial cells were pretreated for 2 h with R-TBZ (10 μM), parent compounds (RESV and TBZ; 10 μM) or vehicle (VEH) and then stimulated with Der P1 (10 ng/mL, 24 h) **(A)** Representative immunofluorescence staining for α-SMA localization (40x objective). **(B)** Semi-quantitative determination (ImageJ/Fiji software) for α-SMA. **(C)** RT-PCR analyses ($2^{-\Delta Ct}$) for the expression of α-SMA-codifying gene. Data are expressed as mean ± S.E.M.; n = 3 **(A, B),** and n = 5 for each group **(C)**. $^{\#}p < 0.05$, $^{\#\#\#}p < 0.001$ *versus* CTR; $^{**}p < 0.01$, $^{***}p < 0.001$ *versus* vehicle (VEH). Statistical analysis used: ordinary one-way ANOVA plus Dunnett's *post hoc* test.

anti-Mouse IgG (Jackson ImmunoResearch, 1:500) for 1 h at room temperature. Colour development was visualized using 3,3'-diaminobenzidine Chromogen Solution (SIGMAFAST™-DAB). Images were acquired with Leica DM RB microscope (Leica, Milan, Italy) using a 20x objective

2.3.5. IgE and cytokine evaluation

Blood was collected by intracardiac puncture using citrate as anticoagulant. Then plasma was obtained by centrifugation at 800 x g at 4 °C for 10 min and immediately frozen at −80 °C. Total IgE levels were measured through an ELISA test using matched antibody pairs (BD Biosciences Pharmingen San Jose, CA). Lungs were isolated and homogenized in ice-cold PBS pH 7.4 (100 mg mL^{-1}, Sigma Aldrich, Milan, Italy) using a FastPrep tissue homogenizer (2 cycles of 20 sec, 6 m/s; MP Biomedicals, DBA, Segrate, Italy). The homogenate was centrifuged (4 °C, 6000 × g, 10 min). Commercially available ELISA test was used to measure the levels of IL-13 and IL-4 (DuoSet ELISA R&D systems).

2.4. Statistical analysis

The results are expressed as mean ± S.E.M of the mean of *n* observations, where n represents the number of animals or number of experiments performed on different days. In the experiments involving histology, the figures shown are representative of six animals.

Statistical evaluation was performed by using unpaired *t*-test or one-way or two-way ANOVA followed by Dunnett's post hoc test by using GraphPad Instant (Graphpad Software Inc., San Diego, CA). A significance threshold of $p < 0.05$ was used.

3. Results

3.1. R-TBZ synthesized via microwave-assisted green chemistry shows high stability and predictable enzymatic activation

The H_2S donor scaffold TBZ-COOH and the final compound R-TBZ hybrid were synthesized using the strategies depicted in Fig. 1 A. The intermediate TBZ-COOH was synthesized from commercially available 4-cyanobenzoic acid via thionation with P_4S_{10}, following previously reported [24] procedures with suitable modifications. Notably, both the thionation step and the subsequent esterification of the 4′-hydroxyl group of RESV with the intermediate TBZ-COOH were performed under microwave-assisted conditions to reduce reaction times, increase yields, and adhere to the principles of green chemistry. To evaluate the chemical and enzymatic stability of the novel hybrid molecule under biologically relevant conditions, R-TBZ was incubated at 37 °C in two media: phosphate-buffered saline (PBS, pH 7.4) to simulate blood

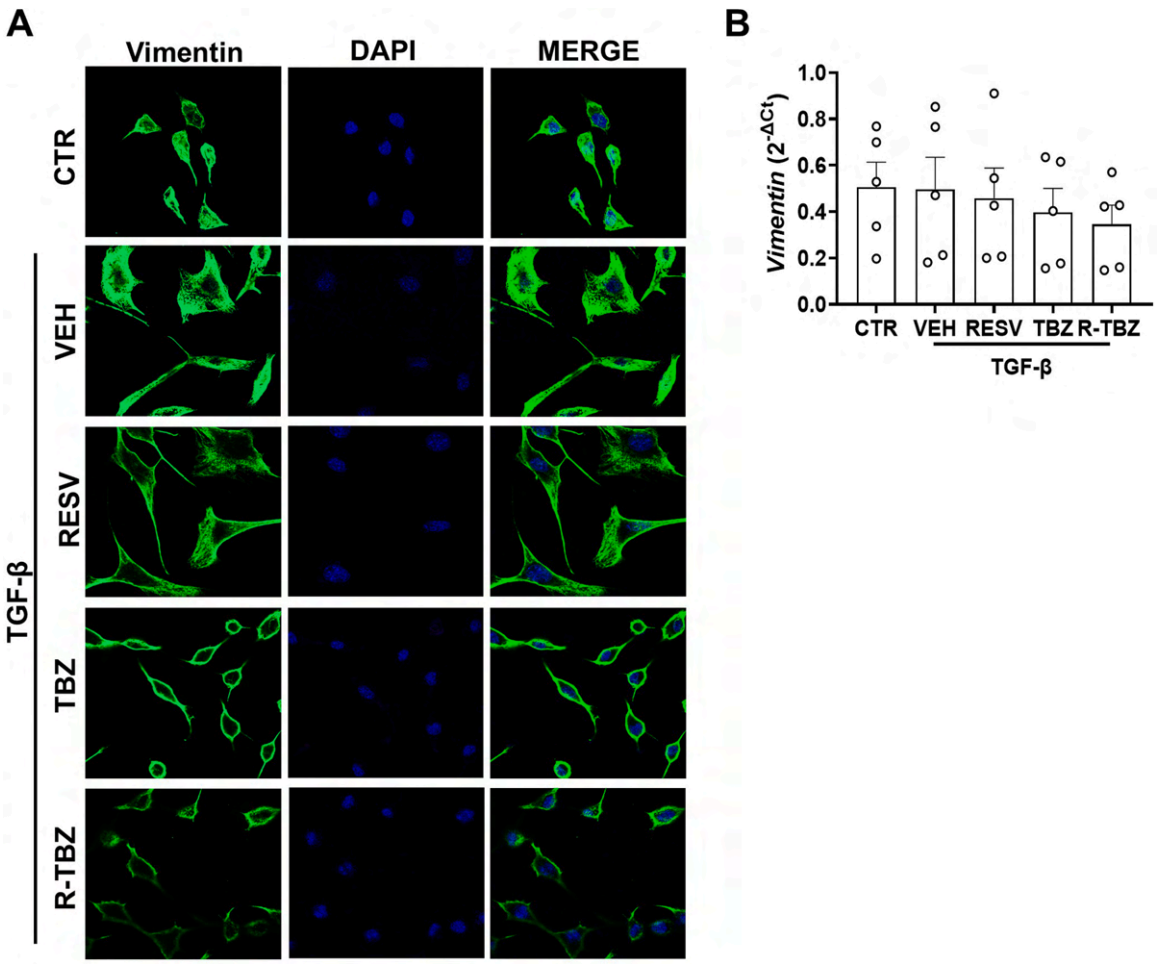

Fig. 5. R-TBZ inhibits fibroblast-to-myofibroblast differentiation (FMD). NIH 3T3 cells were pretreated with R-TBZ (10 μM), the parent compounds (RESV and TBZ; 10 μM) or vehicle (VEH) and then stimulated with TGF-β (10 ng/mL, 48 h). **(A)** Representative immunofluorescence staining for α-SMA localization (40x objective). **(B)** RT-PCR analyses ($2^{-\Delta Ct}$) for the expression of α-SMA -codifying gene. Data are expressed as mean ± S.E.M.; n = 3 **(A)** and n = 5 for each group **(B).**

plasma, and simulated gastric fluid (SGF, pH 1.2, without pepsin) to mimic the acidic environment of the stomach. After 24 h, less than 5 % of R-TBZ has degraded in either condition, indicating over 95 % of the compound remained intact. These findings demonstrate excellent chemical stability across a broad pH range and highlight the robustness conferred by the molecular hybridization strategy. Importantly, the only degradation product detected under these conditions was the parent compound RESV, suggesting that hydrolysis, when it occurs, proceeds via a predictable and selective pathway, without formation of undesired secondary metabolites. Given that R-TBZ is designed as a multi-target compound, its enzymatic cleavage is critical for therapeutic activity. To assess this, the compound was incubated at 37 °C in an esterase-rich environment using bovine serum albumin (BSA). Quantification was carried out using the same validated chromatographic method employed in the chemical stability study. Under these conditions, R-TBZ underwent gradual enzymatic hydrolysis, releasing free RESV over time. The calculated *half-life* ($t_{1/2}$) was approximately 20 h, reflecting a moderate rate of hydrolysis and supporting the concept of controlled, prolonged release of the active components *in vitro*. Overall, these results demonstrate that R-TBZ possesses chemical and enzymatic stability compatible with sustained release, highlighting its potential for *vivo* applications and warranting further pharmacokinetic evaluation. A summary of the chemical and enzymatic stability findings is presented in Fig. 1B.

3.2. R-TBZ abrogates allergen-induced epithelial responses

Epithelial cells, BEAS-2B, were pre-treated for 2 h with R-TBZ (10 μM), the parent compounds (10 μM) or vehicle (DMSO 0.5 %) and then stimulated with Der P1 (10 ng/mL, 24 h). Expression levels of antioxidant enzymes (SOD2, GPX), mucin (MUC5AC), and inflammatory cytokines (IL-6, IL-1β and TNF-α) were assessed. R-TBZ treatment increased the expression of *SOD2*, (Fig. 2 A) and reduced *GPXI* levels (Fig. 2B), suggesting a potential shift in antioxidant pathway preference. A notable decrease in *MUC5AC* expression was observed, indicating reduced mucus production (Fig. 2 C). Furthermore, R-TBZ markedly suppressed the expression of pro-inflammatory cytokines, including IL-6, TNF-α and IL-1β (Fig. 2D, E and F). Accordingly, TBZ (Fig. 2A–F) and RESV (Fig. 2A–F) exhibited similar profiles, but with different efficacy compared to R-TBZ. RT-PCR and immunofluorescence analysis were used to assess the effect of R-TBZ on epithelial-mesenchymal transition (EMT), an event related to airway remodeling. R-TBZ showed a significant inhibitory effect on both allergen-induced vimentin (Fig. 3) and α-SMA upregulation (Fig. 4). This effect was partially reproduced by TBZ, while RESV was less efficacious (Figs. 3 and 4), confirming the synergic effect of the hybrid compound.

3.3. R-TBZ inhibits fibroblast activation and myofibroblast differentiation

Fibroblasts were pretreated with R-TBZ (10 μM), parent compounds (RESV and TBZ; 10 μM) or vehicle (DMSO 0.5 %) and then stimulated

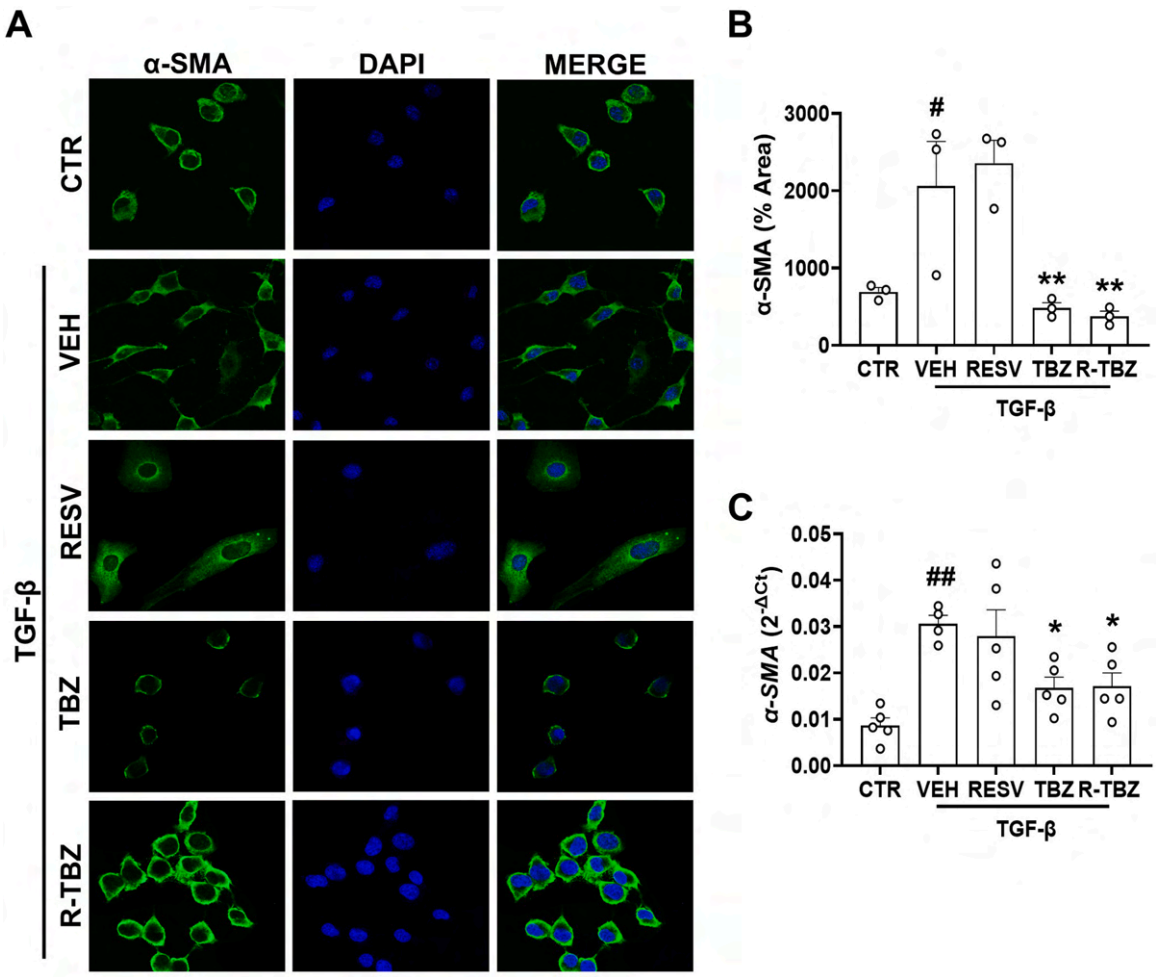

Fig. 6. R-TBZ inhibits fibroblast activation. NIH-3T3 cells were pretreated with R-TBZ (10 μM), the parent compounds (RESV and TBZ; 10 μM) or vehicle (DMSO 0.5 %) and then stimulated with TGF-β (10 ng/mL, 48 h). **(A)** Representative immunofluorescence staining for vimentin localization (40x objective). **(B)** Semi-quantitative determination (ImageJ/Fiji software) for vimentin. **(C)** RT-PCR analyses ($2^{-\Delta Ct}$) for the expression of vimentin-codifying gene. Data are expressed as mean ±SEM; n = 3 **(A, B)** and n = 5 for each group **(C)**. $^{\#}p < 0.05$, $^{\#\#}p < 0.01$ *versus* untreated cell (CTR); *p < 0.05; **p < 0.01 *versus* vehicle (VEH). Statistical analysis used: ordinary one-way ANOVA plus Dunnett's *post hoc* test.

with TGF-β (10 ng/mL, 48 h).

Localization and expression levels of vimentin (Fig. 5) and α-SMA (Fig. 6) were evaluated by immunofluorescence and RT-PCR, respectively. Stimulation with TGF-β significantly shifted vimentin localization from a perinuclear to a cytosolic distribution (Fig. 5) and increased α-SMA (Fig. 6) expression, consistent with the activation of fibroblasts and myofibroblasts differentiation. Co-treatment with R-TBZ significantly reversed both effects, indicating a potent inhibitory effect on the TGF-β–induced fibrotic phenotype. Notably, the hybrid compound demonstrated a synergistic effect.

3.4. *RESV ameliorates airway function but does not prevent airway remodeling*

The effect of RESV on airway function was assessed both *ex vivo* and *in vivo* experiments. In isolated bronchial tissues, cumulative administration of RESV (0.01 mM) demonstrated a bronchodilatory effect (Fig. 7B), although this was not associated with significant changes in bronchial contractility (Fig. 7 A), suggesting direct smooth muscle relaxation rather than modulation of baseline tone. *In vivo*, sensitized mice received intraperitoneal administration of RESV at a dose of 10 mg/kg (Fig. 7 C). RESV significantly attenuated OVA-induced airway hyperresponsiveness (AHR) (Fig. 7D) and restored the bronchial responsiveness to β_2-agonist administration (Fig. 7E). This improvement in airway function was accompanied by a partial reduction in circulating IgE levels (Fig. 7 F), suggesting a modulatory effect on the allergic sensitization process. Allergen exposure triggered substantial Th2 cytokines (IL-13 and IL-4; Fig. 7 G, H) increase, RESV partially mitigated this increase as well as a reduction in IL-13 (Fig. 7 G) and IL-4 (Fig. 7H).

3.5. *R-TBZ exhibits combined anti-inflammatory, antioxidant, and anti-remodeling properties*

Sensitized mice were treated with TBZ at a dose of 5 mg/kg, and key features of asthma were subsequently evaluated. TBZ treatment abrogated AHR (Fig. 8A) and restored bronchial responsiveness to salbutamol, a β_2-adrenergic agonist (Fig. 8B). Similarly, R-TBZ, administered both at 5 mg/kg and 10 mg/kg, produced a comparable effect in normalizing bronchial reactivity (Fig. 8C and D). Immunohistochemical analysis revealed a significant reduction in α-SMA expression in the peribronchial regions of mice treated with either TBZ or R-TBZ, but not with RESV alone (Fig. 8E, F). OVA sensitization induced marked alterations in goblet cells morphology (Fig. 9). These alterations included basal membrane detachment (Fig. 9, asterisk), goblet cell hypertrophy (Fig. 9, arrowhead), and accumulation of mucus and cellular debris in the airway lumen (Fig. 9, arrow), features characteristic of allergic airway inflammation. Pretreatment with RESV partially mitigated these pathological changes, the detachment of the basal lamina is no longer

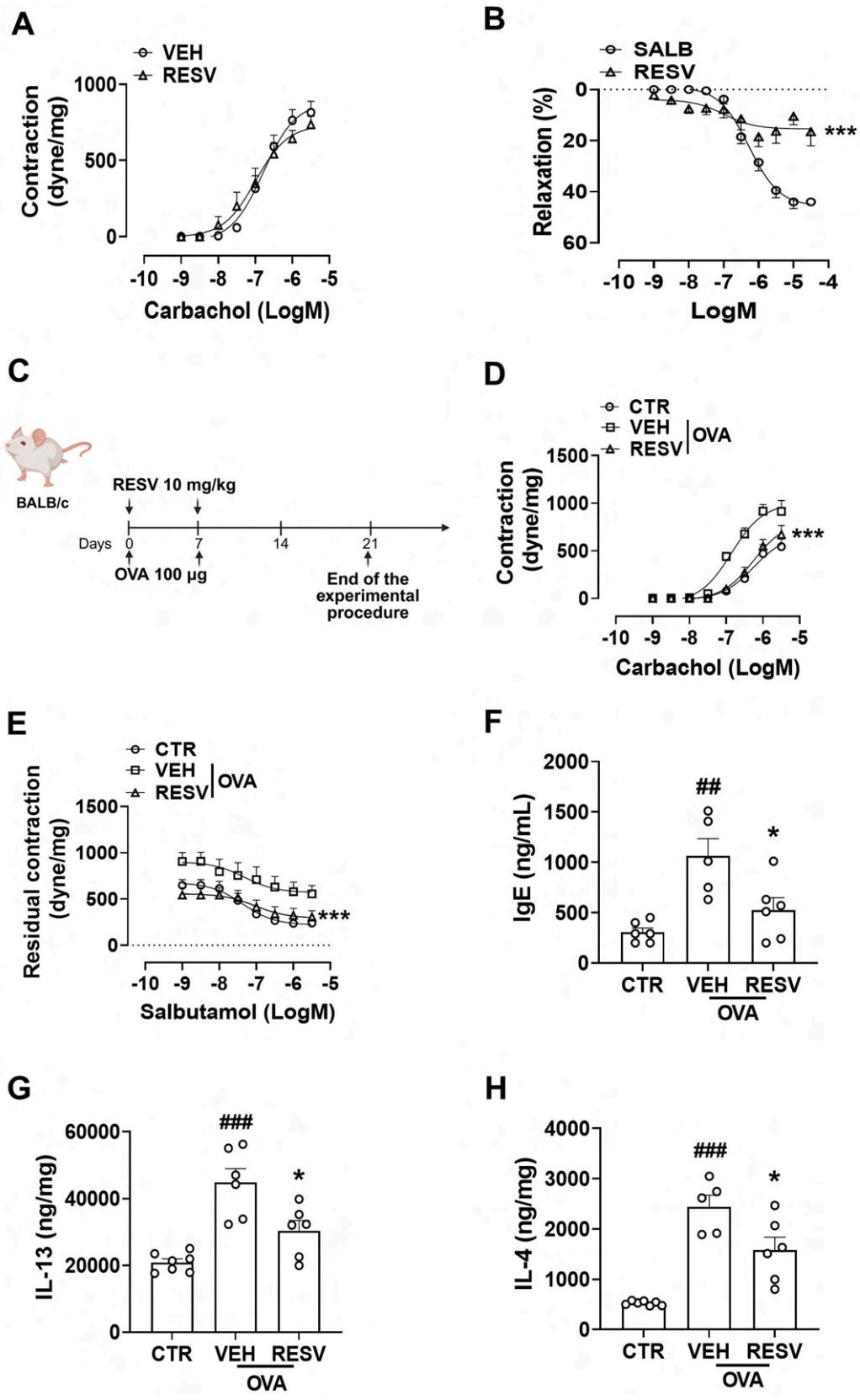

(caption on next page)

Fig. 7. RESV modulates bronchial tone and prevents allergen-induced AHR. **(A)** Bronchial reactivity to carbachol was assessed in the presence of RESV in bronchi harvested from naïve mice. **(B)** Pre-contracted bronchi from naïve mice were stimulated with increasing concentrations of RESV and compared to salbutamol. (**C**) BALB/c mice were sensitized with OVA 100 μg (s.c.) on day 0 and 7, part of these mice were pretreated with RESV (10 mg/kg i.p). Bronchi harvested from sensitized mice were used to measure **(D)** reactivity to carbachol or **(E)** bronchorelaxing response to β_2-agonist. **(F)** Plasma IgE and pulmonary **(G)** IL-13 and **(H)** IL-4 levels were measured by ELISA test. Data are expressed as mean ± S.E.M.; n = 6 **(A-H)** for each group. $^{\#\#}p < 0.01$, $^{\#\#\#}p < 0.001$ *versus untreated cells* (CTR); $^{*}p < 0.05$; $^{**}p < 0.01$, $^{***}p < 0.001$ *versus vehicle* (VEH). Statistical analysis used: two-way ANOVA plus Bonferroni *post hoc* test **(D, E)**, ordinary one-way ANOVA plus Dunnett's *post hoc* test **(F, G, H)**.

visible, but the goblet cells have an enlarged apical portion. PAS^+ staining further supported TBZ's contribution to the protective effects of the hybrid.

R-TBZ treatment markedly improved goblet cell morphology, as demonstrated by reduced goblet cell hypertrophy and diminished basement membrane detachment (Fig. 9). These findings underscore the superior efficacy of R-TBZ in mitigating both functional and structural features of allergic airway inflammation, as further supported by H&E staining and serum IgE quantification (Fig. 10A–C). OVA sensitization also induced marked histological alterations, such as apical enlargement of epithelial cells (Fig. 10A, arrow), alveolar septal thickening (Fig. 10A, asterisk), and alveolar collapse (Fig. 10A, arrowhead). RESV pretreatment partially preserved epithelial structure (Fig. 10A, arrow), reducing septal thickening and alveolar collapse (Fig. 10A, asterisk and arrowhead) and decreasing eosinophilic infiltration (Fig. 10B) as well as IgE plasma level (Fig. 10C). R-TBZ demonstrated a synergistic effect in restoring lung structure in a dose-dependent manner (Fig. 10A, B) as well as IgE plasma level (Fig. 10C).

The synergistic anti-inflammatory effect of R-TBZ was corroborated *in vitro* using LPS-activated J774 macrophages. While both RESV and TBZ individually reduced the production of inflammatory mediators nitric oxide (NO, Fig. 10D) and prostaglandin E_2 (PGE_2, Fig. 10E), R-TBZ demonstrated a greater inhibitory effect, recapitulating and amplifying the activity of the parent compounds.

4. Discussion

In this study, we present a novel RSV hybrid compound, R-TBZ, synthesized by esterification of the 4′-hydroxyl group of RESV with TBZ, a well-characterized slow-releasing H_2S donor. The rationale underlying this hybrid design is to chemically integrate the antioxidant and anti-inflammatory properties of RESV with the controlled and sustained H_2S-releasing capacity of TBZ, thereby improving chemical stability, pharmacodynamic performance, and therapeutic efficacy. The hybrid compound demonstrated excellent chemical stability and showed an improved pharmacological profile compared to its parent compounds in managing asthma-related features, particularly airway remodeling. The molecular design aims to prolong RESV activity, while enabling controlled H_2S release, thus minimizing the risks associated with fast-releasing H_2S donors, and overcoming the intrinsic limitations of RESV in clinical applications, such as poor bioavailability and rapid metabolic inactivation.

Airway remodeling is a progressive and often irreversible pathological hallmark of chronic asthma, contributing to declining lung function and reduced responsiveness to standard anti-inflammatory therapies [25]. While corticosteroids remain the cornerstone of asthma management, their limited efficacy in reversing structural changes—such as airway smooth muscle hypertrophy, subepithelial fibrosis, epithelial disruption, and goblet cell hyperplasia—underscores the urgent need for novel therapeutics that target both inflammation and remodeling simultaneously [26,27]. H_2S, a gaseous signaling molecule endogenously synthesized in the respiratory system, has emerged as a potential modulator of airway remodeling. Several studies have demonstrated that H_2S donors can attenuate key features of airway remodeling in experimental models of asthma, including ASM hyperplasia, subepithelial fibrosis, and inflammatory cell infiltration [28,29]. Despite its therapeutic promise, the clinical translation of H_2S has been hindered by the unfavorable pharmacokinetics and toxicity profile of simple sulfide salts. This has driven the development of novel H_2S-releasing compounds with controlled release kinetics, which, when combined with pharmacologically active molecules through hybridization strategies, can function as multi-target therapeutic agents.

The development of the R-TBZ hybrid represents a promising pharmacological strategy. This molecular design aims not only to overcome the pharmacokinetic limitations of RESV, such as poor bioavailability and rapid metabolism, but also to introduce H_2S-mediated beneficial effects, thereby expanding the therapeutic scope of RESV to include anti-remodeling activity. To achieve this, the 4′-hydroxyl group of RESV, one of the main sites of metabolic inactivation, was selectively blocked via esterification, an approach previously applied successfully in other RESV derivatives to enhance stability and biological performance [30]. Our chemical and enzymatic stability studies demonstrate that R-TBZ is highly stable under both neutral (PBS, pH 7.4) and acidic (SGF, pH 1.2) conditions, with less than 5 % degradation over 24 h. In these conditions, the only detectable degradation product was RESV, indicating a predictable and selective hydrolysis pathway without formation of toxic byproducts. Enzymatic cleavage in an esterase-rich environment confirmed the compound's capability for controlled biotransformation, with a calculated half-life of approximately 20 h. These properties support the suitability of R-TBZ for sustained vivo exposure, a critical requirement for chronic airway diseases that require long-term management.

Functionally, our data highlights an enhanced efficacy profile of the R-TBZ hybrid compared to the individual parent compounds. When evaluated in hybrid form, R-TBZ displayed integrated pharmacological effects attributable to both RESV and TBZ. First, we evaluated its activity in an in vitro model of allergic airway inflammation involving epithelial cell activation, oxidative stress, mucus hypersecretion, and pro-inflammatory cytokine release. Epithelial cells were treated with allergen stimulation in the presence or absence of R-TBZ and compared with parent compounds. R-TBZ treatment increased the expression of SOD2, indicating enhanced mitochondrial antioxidant defense. Conversely, GPX1 levels were reduced, suggesting a shift in antioxidant pathway utilization. A marked decrease in MUC5AC expression was also observed, indicating reduced mucus production. Furthermore, R-TBZ significantly suppressed the expression of pro-inflammatory cytokines, including IL-6, IL-1β, and TNF-α. Notably, these effects were achieved at lower concentrations than those required for RESV or TBZ alone, supporting an improved pharmacodynamic efficiency of the hybrid compound. Similar results were obtained in TGF-β–stimulated fibroblasts, where R-TBZ inhibited fibroblast activation and myofibroblast differentiation, as evidenced by a significant reduction in α-SMA and vimentin expression. These anti-fibrotic effects were largely attributable to the TBZ moiety, as TBZ alone exerted comparable inhibitory activity, whereas RESV showed limited efficacy under these conditions.

Consistent findings were observed in an in vivo experimental model of allergic asthma. RESV alone, at higher doses, exhibited significant anti-inflammatory activity, as demonstrated by reduced airway hyperresponsiveness (AHR), improved β_2-agonist responsiveness, and a partial decrease in circulating IgE levels in OVA-sensitized mice. Histologically, RESV preserved epithelial architecture and reduced mucus hypersecretion, eosinophilic infiltration, and Th2 cytokine levels (IL-4 and IL-13). However, RESV did not significantly modulate α-SMA expression, a marker of airway smooth muscle remodeling. This limitation is particularly relevant, as ASM hyperplasia represents one of the most refractory components of airway remodeling and is strongly associated with poor

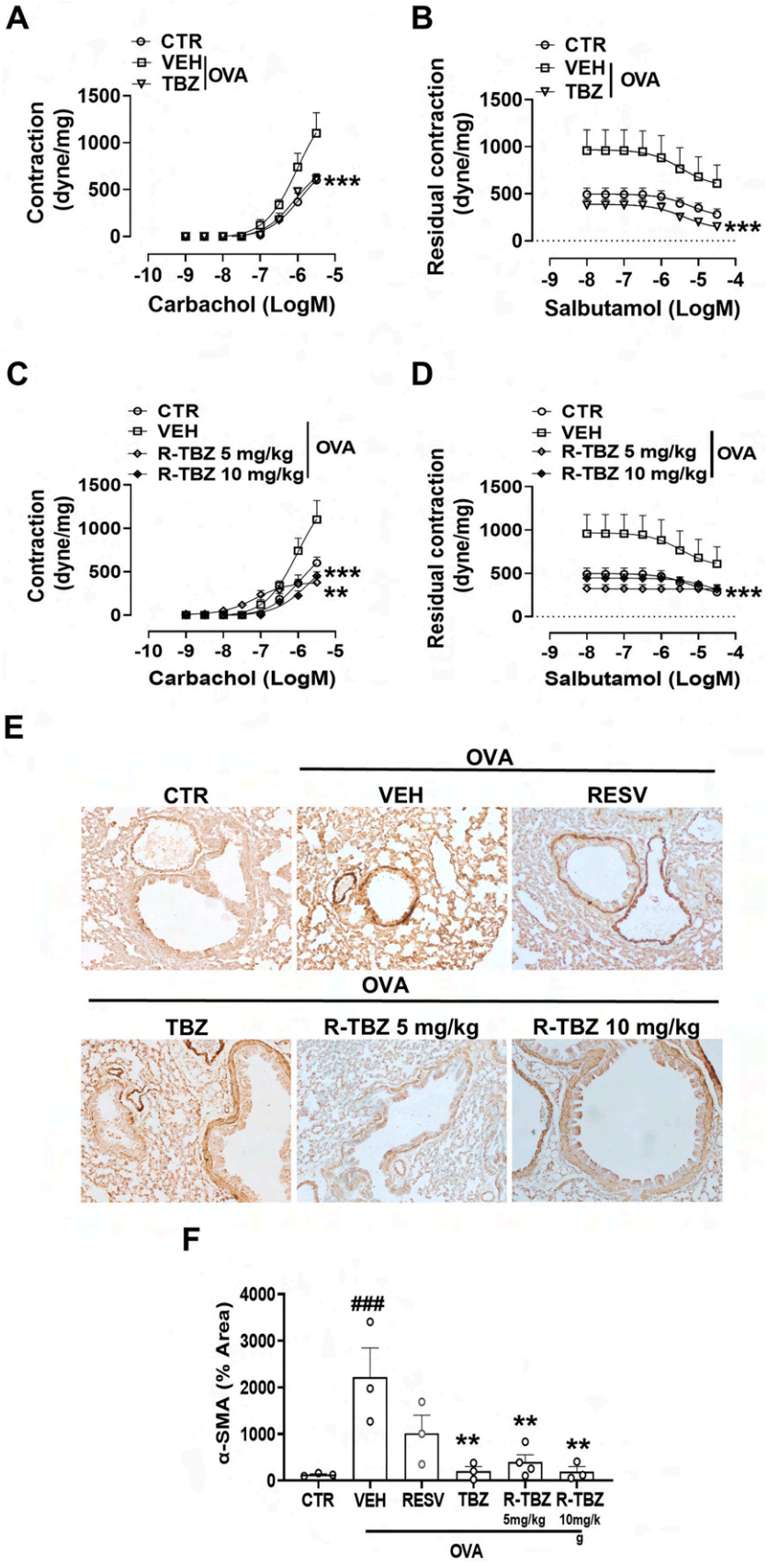

(caption on next page)

Fig. 8. R-TBZ exhibits a synergistic effect in asthma features management. BALB/c mice were pretreated with TBZ 5 mg/kg, RESV 10 mg/kg, and R-TBZ 5 or 10 mg/kg, or vehicle (saline) and then sensitized with OVA 100 μg (s.c.) on days 0 and 7. Bronchi were harvested from treated mice and then exposed to **(A, C)** carbachol or **(B, D)** salbutamol. **(E)** Representative IHC images of α-SMA localization in the lung (20x objective). **(F)** Semi-quantitative determination for α-SMA in the lung section. Data are expressed as mean ± S.E.M.; n = 6 for each group. $^{###}p < 0.001$ *versus control mice* (CTR); $^{**}p < 0.01$, $^{***}p < 0.001$ *versus* VEH/OVA. Statistical analysis used: two-way ANOVA plus Bonferroni *post hoc* test **(A-D)**, ordinary one-way ANOVA plus Dunnett's *post hoc* test **(F)**.

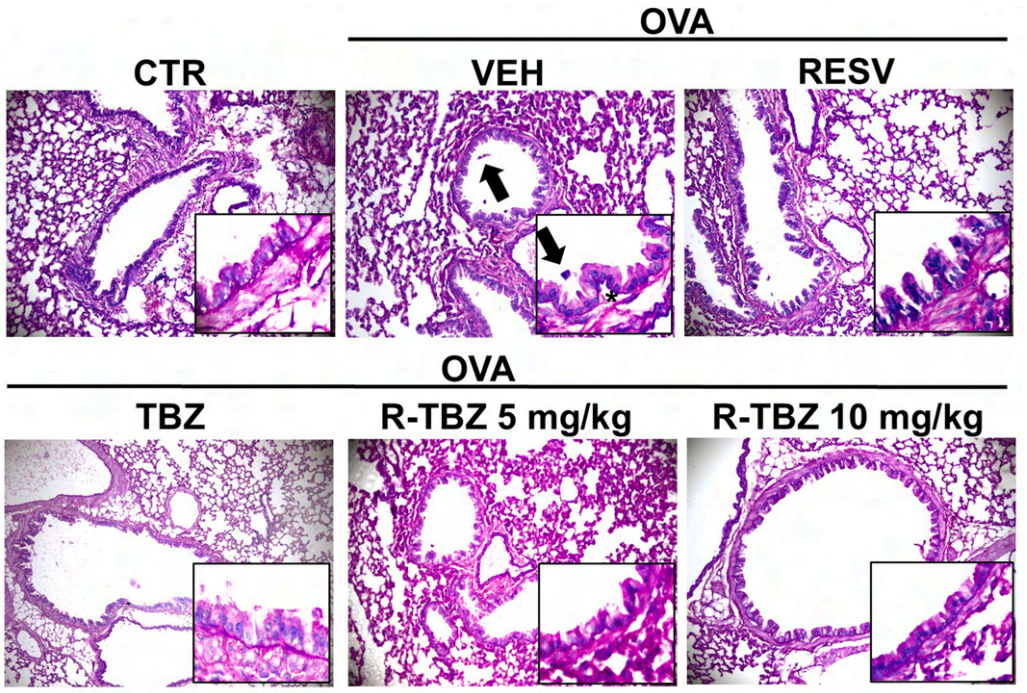

Fig. 9. R-TBZ restores goblet cells morphology *in vivo*. BALB/c mice were pretreated with TBZ 5 mg/kg, RESV 10 mg/kg, R-TBZ 5 or 10 mg/kg, or vehicle (saline) and then sensitized with OVA 100 μg (s.c.) on days 0 and 7 10 min before each OVA administration. Representative image for PAS^{+} staining in lung sections of treated mice (10x objective, insert with 20x objective).

clinical outcomes. In contrast, TBZ exerted a pronounced effect on airway remodeling, significantly reducing AHR, restoring bronchodilatory responsiveness, and decreasing peri-bronchial α-SMA expression, suggesting a direct anti-remodeling activity mediated by H_2S release. These observations are in line with previous studies indicating that H_2S modulates fibrotic and remodeling processes through inhibition of TGF-β1/Smad signaling, attenuation of oxidative stress, and regulation of redox-sensitive inflammatory pathways.

Importantly, the R-TBZ hybrid integrated the beneficial effects of both RESV and TBZ, resulting in a broader and more consistent amelioration of asthma-related features. Compared with RESV alone, R-TBZ demonstrated superior efficacy in reducing airway remodeling markers and improving lung function parameters, particularly at lower doses, suggesting increased potency and pharmacodynamic synergy. In vivo, R-TBZ attenuated allergen-induced AHR, reduced α-SMA expression, and restored epithelial integrity more effectively than either parent compound. Histological analysis further revealed preservation of goblet cell morphology and basement membrane structure, alongside a marked reduction in IgE levels and eosinophilic infiltration, highlighting the dual impact of the hybrid compound on both immune-driven inflammation and structural remodeling. These findings are particularly significant given that airway remodeling often progresses independently of inflammation and is typically resistant to corticosteroid therapy [31]. The contribution of TBZ via controlled H_2S release offers a mechanistically plausible and therapeutically relevant approach to targeting this unmet clinical need. Moreover, the slow and sustained release of H_2S from the TBZ moiety likely mitigates the cytotoxicity associated with rapid-release H_2S donors, providing a safer and more physiologically compatible strategy for chronic intervention.

Nevertheless, several limitations should be acknowledged. Although TBZ and R-TBZ showed marked efficacy in these experimental models, direct causal validation of H_2S-mediated mechanisms (e.g., rescue experiments with H_2S inhibitors or quantification of protein S-sulfhydration) was not feasible and remains to be addressed in future studies. Additionally, while R-TBZ demonstrated favorable stability and bioactivity under the tested conditions, its long-term safety profile and pharmacokinetic behavior require further investigation. Comprehensive toxicological assessments and chronic asthma models will be essential to fully define the translational potential of this compound. A further limitation to the generalizability of the study is that it did not consider gender/sex issues.

In conclusion, the R-TBZ hybrid exemplifies a rational drug design strategy aimed at overcoming the pharmacokinetic limitations of RESV while integrating the pleiotropic protective effects of H_2S. Its dual anti-inflammatory and anti-remodeling activity, together with improved stability and efficacy at lower doses, positions R-TBZ as a promising preclinical candidate for the treatment of asthma and potentially other chronic inflammatory airway diseases. The contribution of TBZ, both as

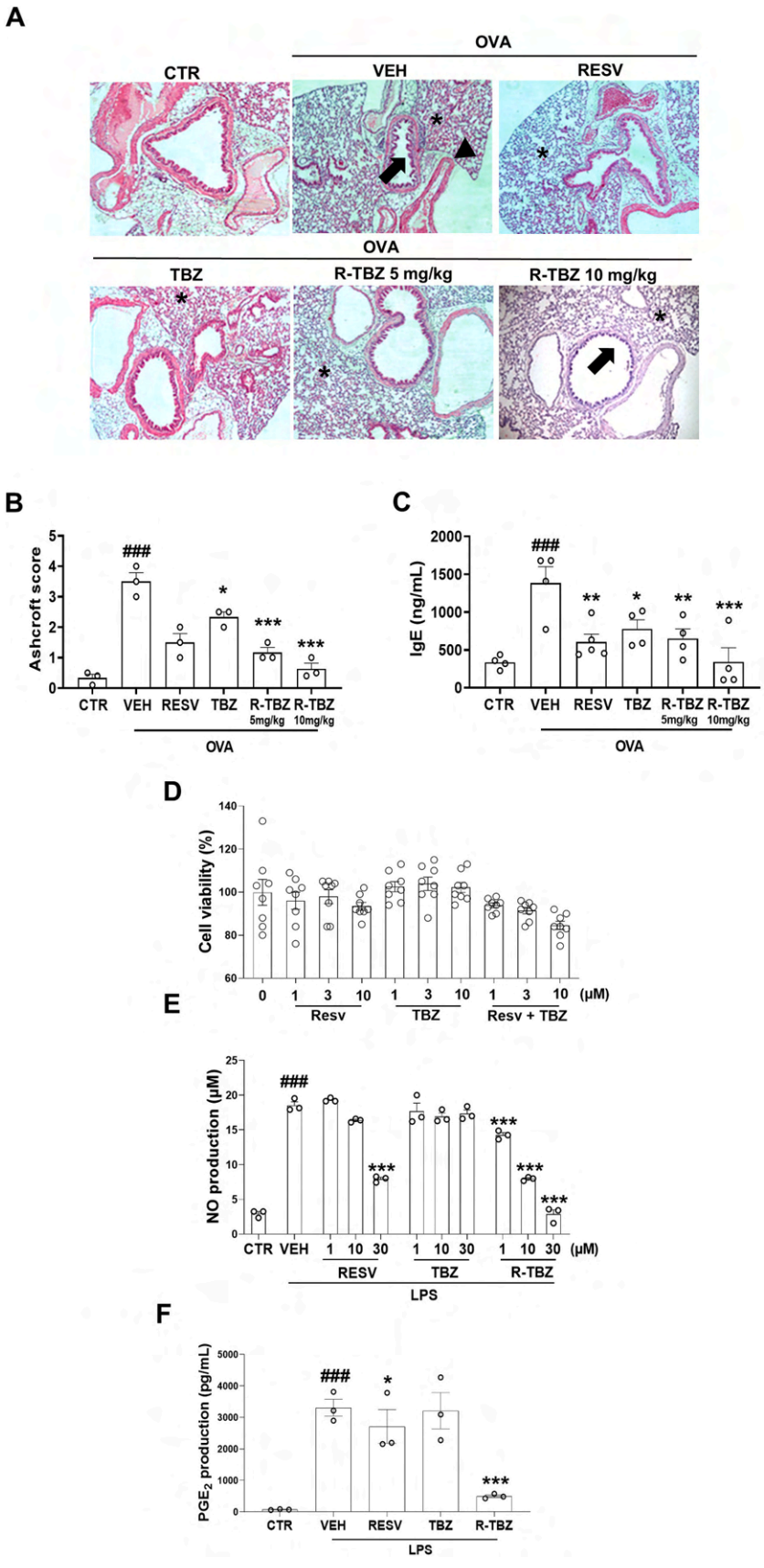

(caption on next page)

Fig. 10. R-TBZ reduces OVA-induced lung injury. BALB/c mice were pretreated with TBZ 5 mg/kg, RESV 10 mg/kg, R-TBZ 5 or 10 mg/kg, or vehicle (saline) and then sensitized with OVA 100 μg (s.c.) on days 0 and 7. **(A)** Representative images of H&E staining of lung sections (10x objective). **(B)** Lung inflammation was quantified by using Ashcroft score, which ranges from 0 (no inflammation) to 4 (severe inflammation). **(C)** IgE levels were evaluated on plasma. **(D)** Cells were pretreated for 24 h with RESV, TBZ, or R-TBZ (1–3–10 μM), and cell viability was evaluated by the mitochondrial-dependent reduction of MTT to formazan. **(E)** J774 cells were pretreated for 2 h with RESV, TBZ or R-TBZ (1, 3, 10 μM) and then stimulated for 24 h with LPS (10 μg/mL) to evaluate supernatans level of nitrite. **(F)** J774 cells were pretreated for 2 h with RESV, TBZ or R-TBZ (10 μM) and then stimulated for 24 h with LPS (10 μg/mL) to evaluate supernatans level of PGE_2. Data are expressed as mean ± S.E.M.; n = 3 **(A, B, D, E)** for each group, n = 6 **(C)** for each group. $^{###}p < 0.001$ *versus untreated cell* (CTR); *p < 0.05; **p < 0.01; ***p < 0.001 *versus vehicle* (VEH). Statistical analysis used: ordinary one-way ANOVA plus Dunnett's *post hoc* test.

a standalone agent and within the hybrid structure, is particularly noteworthy for its ability to target airway remodeling, a major therapeutic gap in current asthma management.

CRediT authorship contribution statement

Raffaele Capasso: Writing – review & editing, Methodology. **Antonietta Rossi:** Writing – review & editing, Methodology, Investigation. **Sara Perna:** Methodology, Investigation. **Beatrice Severino:** Writing – review & editing, Methodology, Investigation. **D'Avino Danilo:** Methodology, Investigation. **Giuseppe Caliendo:** Writing – review & editing, Methodology, Investigation. **Ida Cerqua:** Writing – original draft, Project administration, Methodology, Investigation, Formal analysis, Conceptualization. **Alessandra Perrella:** Methodology, Investigation. **Fiorentina Roviezzo:** Writing – review & editing, Validation, Resources, Investigation, Formal analysis, Conceptualization. **Elisabetta Granato:** Methodology, Investigation. **Angela Corvino:** Writing – review & editing, Methodology. **Antonia Scognamiglio:** Methodology, Investigation. **Federica Sodano:** Methodology, Investigation. **Ferdinando Fiorino:** Writing – original draft, Methodology, Investigation. **Martina Simonelli:** Methodology, Investigation, Data curation. **Elisa Magli:** Methodology, Investigation.

Acknowledgement

This work was supported by Ministero dell'Università e della Ricerca (MIUR) PRIN 2022MMSBKL.

Declaration of Competing Interest

The authors declare that they have no known competing financial interests or personal relationships that could have appeared to influence the work reported in this paper.

Data availability

Data will be made available on request.

References

[1] S. Weiskirchen, R. Weiskirchen, Resveratrol: how much wine do you have to drink to stay healthy? Adv. Nutr. 7 (4) (2016) 706–718.
[2] J.A. Baur, D.A. Sinclair, Therapeutic potential of resveratrol: the in vivo evidence, Nat. Rev. Drug Discov. 5 (6) (2006) 493–506.
[3] A.R. Martin, I. Villegas, C. La Casa, C.A. de la Lastra, Resveratrol, a polyphenol found in grapes, suppresses oxidative damage and stimulates apoptosis during early colonic inflammation in rats, Biochem. Pharm. 67 (7) (2004) 1399–1410.
[4] R.H. Wong, N.M. Berry, A.M. Coates, J.D. Buckley, J. Bryan, I. Kunz, P.R. Howe, Chronic resveratrol consumption improves brachial flow-mediated dilatation in healthy obese adults, J. Hypertens. 31 (9) (2013) 1819–1827.
[5] V.A. Brown, K.R. Patel, M. Viskaduraki, J.A. Crowell, M. Perloff, T.D. Booth, G. Vasilinin, A. Sen, A.M. Schinas, G. Piccirilli, K. Brown, W.P. Steward, A. J. Gescher, D.E. Brenner, Repeat dose study of the cancer chemopreventive agent resveratrol in healthy volunteers: safety, pharmacokinetics, and effect on the insulin-like growth factor axis, Cancer Res. 70 (22) (2010) 9003–9011.
[6] H.A. Hausenblas, J.A. Schoulda, J.M. Smoliga, Resveratrol treatment as an adjunct to pharmacological management in type 2 diabetes mellitus–systematic review and meta-analysis, Mol. Nutr. Food Res. 59 (1) (2015) 147–159.
[7] A.P. Majumdar, S. Banerjee, J. Nautiyal, B.B. Patel, V. Patel, J. Du, Y. Yu, A. A. Elliott, E. Levi, F.H. Sarkar, Curcumin synergizes with resveratrol to inhibit colon cancer, Nutr. Cancer 61 (4) (2009) 544–553.
[8] H.H. Chow, L.L. Garland, C.H. Hsu, D.R. Vining, W.M. Chew, J.A. Miller, M. Perloff, J.A. Crowell, D.S. Alberts, Resveratrol modulates drug- and carcinogen-metabolizing enzymes in a healthy volunteer study, Cancer Prev Res. (Phila) 3 (9) (2010) 1168–1175.
[9] P. Brasnyo, G.A. Molnar, M. Mohas, L. Marko, B. Laczy, J. Cseh, E. Mikolas, I. A. Szijarto, A. Merei, R. Halmai, L.G. Meszaros, B. Sumegi, I. Wittmann, Resveratrol improves insulin sensitivity, reduces oxidative stress and activates the Akt pathway in type 2 diabetic patients, Br. J. Nutr. 106 (3) (2011) 383–389.
[10] L.M. Howells, D.P. Berry, P.J. Elliott, E.W. Jacobson, E. Hoffmann, B. Hegarty, K. Brown, W.P. Steward, A.J. Gescher, Phase I randomized, double-blind pilot study of micronized resveratrol (SRT501) in patients with hepatic metastases–safety, pharmacokinetics, and pharmacodynamics, Cancer Prev Res. (Phila) 4 (9) (2011) 1419–1425.
[11] R. Kala, H.N. Shah, S.L. Martin, T.O. Tollefsbol, Epigenetic-based combinatorial resveratrol and pterostilbene alters DNA damage response by affecting SIRT1 and DNMT enzyme expression, including SIRT1-dependent gamma-H2AX and telomerase regulation in triple-negative breast cancer, BMC Cancer 15 (2015) 672.
[12] J. Gambini, M. Ingles, G. Olaso, R. Lopez-Grueso, V. Bonet-Costa, L. Gimeno-Mallench, C. Mas-Bargues, K.M. Abdelaziz, M.C. Gomez-Cabrera, J. Vina, C. Borras, Properties of resveratrol: in vitro and in vivo studies about metabolism, bioavailability, and biological effects in animal models and humans, Oxid. Med Cell Longev. 2015 (2015) 837042.
[13] M. Urpi-Sarda, R. Zamora-Ros, R. Lamuela-Raventos, A. Cherubini, O. Jauregui, R. de la Torre, M.I. Covas, R. Estruch, W. Jaeger, C. Andres-Lacueva, HPLC-tandem mass spectrometric method to characterize resveratrol metabolism in humans, Clin. Chem. 53 (2) (2007) 292–299.
[14] H. Badie, H. Abbas, Novel small self-assembled resveratrol-bearing cubosomes and hexosomes: preparation, charachterization, and ex vivo permeation, Drug Dev. Ind. Pharm. 44 (12) (2018) 2013–2025.
[15] P. Jeandet, E. Sobarzo-Sanchez, M.S. Uddin, R. Bru, C. Clement, C. Jacquard, S. F. Nabavi, M. Khayatkashani, G.E. Batiha, H. Khan, I. Morkunas, F. Trotta, A. Matencio, S.M. Nabavi, Resveratrol and cyclodextrins, an easy alliance: applications in nanomedicine, green chemistry and biotechnology, Biotechnol. Adv. 53 (2021) 107844.
[16] W.M. Wang, Y. Liu, P. Pan, Y.Q. Huang, T. Chen, T.Y. Yuan, Y.L. Ma, G. Han, J. H. Li, Y.G. Jin, F. Xie, Pulmonary delivery of resveratrol-β-cyclodextrin inclusion complexes for the prevention of zinc chloride smoke-induced acute lung injury, Drug Deliv. 29 (1) (2022) 1122–1131.
[17] R. Guan, J. Wang, D. Li, Z. Li, H. Liu, M. Ding, Z. Cai, X. Liang, Q. Yang, Z. Long, L. Chen, W. Liu, D. Sun, H. Yao, W. Lu, Hydrogen sulfide inhibits cigarette smoke-induced inflammation and injury in alveolar epithelial cells by suppressing PHD2/HIF-1alpha/MAPK signaling pathway, Int. Immunopharmacol. 81 (2020) 105979.
[18] I. Cerqua, E. Granato, A. Corvino, B. Severino, D.D. Avino, M. Simonelli, E. Perissutti, A. Scognamiglio, D. Mirra, B.D. Agostino, G. Caliendo, A. Rossi, G. Cirino, C.M. Motta, F. Roviezzo, Prednisone-hydrogen sulfide releasing hybrid shows improved therapeutic profile in asthma, Front. Pharm. 14 (2023) 1266934.
[19] A. Martelli, L. Testai, V. Citi, A. Marino, I. Pugliesi, E. Barresi, G. Nesi, S. Rapposelli, S. Taliani, F. Da Settimo, M.C. Breschi, V. Calderone, Arylthioamides as H2S donors: l-cysteine-activated releasing properties and vascular effects in vitro and in vivo, ACS Med. Chem. Lett. 4 (10) (2013) 904–908.
[20] J.L. Wallace, G. Caliendo, V. Santagada, G. Cirino, Markedly reduced toxicity of a hydrogen sulphide-releasing derivative of naproxen (ATB-346), Br. J. Pharm. 159 (6) (2010) 1236–1246.
[21] G. Romeo, V. Ciaffaglione, E. Amata, M. Dichiara, L. Calabrese, L. Vanella, V. Sorrenti, S. Grosso, A.G. D'Amico, V. D'Agata, S. Intagliata, L. Salerno, Combination of heme oxygenase-1 inhibition and sigma receptor modulation for anticancer activity, Molecules 26 (13) (2021).
[22] A. Corvino, V. Citi, F. Fiorino, F. Frecentese, E. Magli, E. Perissutti, V. Santagada, V. Calderone, A. Martelli, E. Gorica, S. Brogi, F.F. Colombo, C.N. Capello, H. H. Araujo Ferreira, M.G. Rimoli, F. Sodano, B. Rolando, F. Pavese, A. Petti, M. N. Muscara, G. Caliendo, B. Severino, H(2)S donating corticosteroids: Design, synthesis and biological evaluation in a murine model of asthma, J. Adv. Res 35 (2022) 267–277.
[23] A. Scognamiglio, I. Cerqua, V. Citi, A. Martelli, J. Spezzini, V. Calderone, M. G. Rimoli, F. Sodano, G. Caliendo, V. Santagada, F. Fiorino, F. Frecentese, E. Perissutti, E. Magli, M. Simonelli, A. Corvino, F. Roviezzo, B. Severino, Isothiocyanate-Corticosteroid Conjugates against asthma: unity makes strength, Eur. J. Med Chem. 275 (2024) 116636.
[24] M. Dichiara, A. Artacho-Cordon, R. Turnaturi, M. Santos-Caballero, R. Gonzalez-Cano, L. Pasquinucci, C. Barbaraci, I. Rodriguez-Gomez, M. Gomez-Guzman, A. Marrazzo, E.J. Cobos, E. Amata, Dual Sigma-1 receptor antagonists and hydrogen sulfide-releasing compounds for pain treatment: design, synthesis, and pharmacological evaluation, Eur. J. Med. Chem. 230 (2022) 114091.

[25] B. Camoretti-Mercado, R.F. Lockey, Airway smooth muscle pathophysiology in asthma, J. Allergy Clin. Immunol. 147 (6) (2021) 1983–1995.
[26] R. Beasley, P. Bruce, C. Houghton, L. Hatter, The ICS/formoterol reliever therapy regimen in asthma: a review, J. Allergy Clin. Immunol. Pr. 11 (3) (2023) 762–772, e1.
[27] E.R. Bleecker, A.N. Menzies-Gow, D.B. Price, A. Bourdin, S. Sweet, A.L. Martin, M. Alacqua, T.N. Tran, Systematic literature review of systemic corticosteroid use for asthma management, Am. J. Respir. Crit. Care Med. 201 (3) (2020) 276–293.
[28] C.M. Bartman, M. Schiliro, M. Helan, Y.S. Prakash, D. Linden, C. Pabelick, Hydrogen sulfide, oxygen, and calcium regulation in developing human airway smooth muscle, FASEB J. 34 (9) (2020) 12991–13004.
[29] Y.H. Chen, W.Z. Yao, J.Z. Gao, B. Geng, P.P. Wang, C.S. Tang, Serum hydrogen sulfide as a novel marker predicting bacterial involvement in patients with community-acquired lower respiratory tract infections, Respirology 14 (5) (2009) 746–752.